Available at: https://doi.org/10.1002/admt.202000328

Real-Time Multi-Ion Detection in the Sweat Concentration Range Enabled by Flexible, Printed and Microfluidics-Integrated Organic Transistor Arrays

Silvia Demuru, Brince Paul Kunnel, and Danick Briand**

S. Demuru, Dr. B. P. Kunnel, Dr. D. Briand
Soft Transducers Laboratory
École Polytechnique Fédérale de Lausanne
Neuchâtel 2000
Switzerland
E-mail: silvia.demuru@epfl.ch, danick.briand@epfl.ch

Keywords: organic transistors, ion sensing, microfluidics, printed sensors, wearables

Abstract

Organic electrochemical transistors (OECTs) show remarkable promise as biosensors, thanks to their high signal amplification, simple architecture, and the intrinsic flexibility of the organic material. Despite these properties, their use for real-time sensing in complex biological fluids, such as human sweat, is strongly limited due to the lack of cross-sensitivity and selectivity studies and the use of rigid and bulky device configurations. Here, the development of a novel flexible microfluidics-integrated platform with an array of printed ion-selective OECTs enables multi-ion detection in a wearable fashion. This is achieved by coating the poly(3,4-ethylene dioxythiophene):polystyrene sulfonate (PEDOT:PSS) channels of the transistors with three different ion-selective membranes (ISMs). Systematic electrical and sensing analysis of the OECTs with ISMs show a minimal impact of the membranes on the electrical and time responses of the transistors while providing high ion selectivity. This work combines for the first time real-time and selective multi-ion detection with an array of inkjet-printed and flexible organic transistors coated with different ISMs, demonstrating state-of-the-art sensing capabilities of ~10 μA dec^{-1} for potassium, sodium, and pH. This flexible OECTs sensing platform paves the way to the next generation devices for continuous electrolytes monitoring in body fluids.

Available at: https://doi.org/10.1002/admt.202000328

1. Introduction

There is a growing interest in wearable non-invasive or minimally invasive devices that can continuously analyze biofluids such as interstitial fluid, tears, saliva or sweat.[1–8] Electrolytes such as sodium and potassium ions (Na^+ and K^+) are of fundamental importance for biological processes, including control of the hydration status, nerve and muscle impulse transmission, osmotic pressure balance and pH regulation.[9–11] The monitoring of electrolyte imbalance in everyday life with a wearable device would help notably to understand, predict and prevent pathologies related to moderate and strong dehydration caused, for instance, by excessive heat, intensive exercise, and harmful working conditions.[12–15] More precisely, in human sweat, the concentration of Na^+ changes between 10–100 mM, it is sweat rate-dependent and associated with dehydration.[3,14,16] K^+ concentration level ranges between 1–18.5 mM with a sweat rate-independent partitioning.[3,16] Also, pH can strongly vary between 3–8 units,[3] with changes associated with dehydration and muscle fatigue.[14,15]

For the next generation of wearable ion sensors, key requirements include mechanical flexibility, simple array patterning for multi-parametric analysis, and microfluidics integration for continuous sampling.[17–23] Conventionally, selective ion measurements are performed using potentiometric two-electrode systems, in which the potential drop between an Ion Selective Membrane (ISM) and a reference electrode is measured.[21,24,25] However, standard potentiometric sensors are difficult to integrate into an array configuration in a microfluidic platform, due to their high output impedance,[18] and the difficult miniaturization of a stable reference electrode.[26–28] Organic electrochemical transistors (OECTs) are an interesting alternative to conventional potentiometric sensors, overcoming some of these limitations.[29]

The OECTs are three-terminal devices (drain, source, and gate), with the source and the drain electrodes connected by a conducting polymeric channel. The organic channel is based on conjugated polymer-polyelectrolyte blends, such as the mainly used poly(3,4-ethylene

dioxythiophene):polystyrene sulfonate (PEDOT:PSS).[22,30–32] This active material enables mixed ionic and electronic charges interaction, with ionic conduction provided by the PSS polyelectrolyte chains and electronic conduction by nanometric-sized PEDOT crystallites.[33–35] In the presence of an electrolyte and once a positive gate voltage is applied, the dissolved cations are injected into the PEDOT:PSS channel. The cations compensate electrostatically the sulfonate anions of the PSS phase, subsequently lowering the drain current (hole de-doping) in the bulk of the layer.[2,29] This technology, without the need for a reference electrode, allows a facile miniaturization.[28,36] Moreover, the mechanical flexibility of the PEDOT:PSS channel,[22,37] the compatibility with digital manufacturing such as inkjet printing,[38–41] and the very low output impedance,[18] make OECTs promising candidates for the development of configurable and wearable sensor arrays. Besides, the device physics results in novel electrical characteristics that were never observed in other types of transistors, both organic and inorganic-based, such as a very high transconductance at very low voltages,[33,42–44] enabling high signal amplification and sensitivity.[9,19,45]

OECTs (PEDOT:PSS-based) on flexible substrates are reported for different bio-sensing applications, including chemical and biochemical sensors on plastic,[18,19,46] elastomeric,[47] and paper substrates.[48] However, several challenges in the development of OECTs for wearable bio-sensing applications still remain, with the main problem being the selectivity to the target analyte.[49] Despite the importance of measurements in complex biological fluids such as human sweat, in which multiple ions and other analytes are present, this issue is still rarely taken into account.

With the use of an ion-selective membrane, only the desired cations will contribute, with a certain selectivity, to the de-doping of the PEDOT:PSS layer.[9,18,50,51] However, the behavior of organic transistors for selective ion sensing has been almost exclusively reported for single devices on rigid substrates,[2,9] with the ISM suspended on an inner electrolyte (liquid or hydrogel). Recently, OECTs made, by a combination of screen printing and lithography, on a

flexible substrate with multiple ISMs (without inner electrolyte) have been presented,[18] however, while focusing on the technological integration, the transfer characteristics and responses in time in presence of the analytes were not studied.

In this work, we demonstrate an array of inkjet-printed flexible OECTs that perform real-time, sensitive and selective detection of potassium (K^+), sodium (Na^+), and hydrogen (H^+) ions at physiologically relevant concentrations. Their PEDOT:PSS channels were coated with three different ionophore-based ion-selective membranes, which were developed to have a minimal impact on the electrical and time responses of the transistors while maintaining high ion selectivity. The proposed array of thin-film transistors was integrated into a flexible microfluidic system, enabling continuous measurements of electrolytes in body fluids.

2. Results and Discussion

2.1 Characterization of the inkjet-printed layers

In this work, organic electrochemical transistors were inkjet-printed on a flexible 125 μm-thick polyimide foil (PI) substrate, using conductive-grade PEDOT:PSS (1 S/cm, 1.3 wt % dispersion in H_2O) for the active layer, and silver nanoparticles ink for the gate, source, and drain electrodes (**Figure 1**). The active organic channel area is 1 x 3 mm^2, with an overlap of ~1 mm^2 to the source and drain contacts. The active gate has a planar on foil configuration with an area of 1 x 1 mm^2 and a ~1 mm gap from the channel. Instead of using floating wires or pellets as external gate electrodes,[9,34,42] the proposed design enables straightforward integration of multiple sensing transistors into microfluidics (Figure 1a,d). The schematics of the cross-sections of the integrated OECTs array are illustrated in Figure S1.

Four layers were printed to obtain a continuous PEDOT:PSS film (Figure S2). The organic layers were post-treated by drop-coating dimethyl sulfoxide (DMSO).[52] DMSO post-treatment strongly improves the PEDOT:PSS electrical conductivity and crystallinity,[53] leading to enhanced electrical characteristics in a transistor configuration.[54] A film thickness of 115 ± 28

nm (n=3) and sheet resistance of 0.96 ± 0.06 kΩ/sq (n=4) (Figure S2) is achieved with the post-treatment and four printed layers. In a printed batch of a total of 52 transistors, 2 had a significantly higher resistance (> 40 %) than the others, possibly due to some defects in the printing layer, leading to a fabrication yield of 96 %. Moreover, we observed after ~20 days that the resistance of the treated PEDOT:PSS layers increased by just ~10 % (Figure S3), while for the untreated layers increased of ~200 % likely due to higher water and oxygen absorption from the air.[55] The silver electrodes exhibit a conductivity of ~15 kS/cm for two printed layers with a thickness of ~200 nm. The mechanical flexibility of the system, hence its wearability, was assessed by attaching the integrated device on curved surfaces of different radii equal to 20, 15, and 10 mm (Figure S4), and by measuring the changes in resistance of the PEDOT:PSS channels. A change of less than 0.1 %, defined as the absolute value of $\frac{R-R_{unbended}}{R_{unbended}} x\ 100$, is reported, showing that the bending of the platform does not significantly change the channel conductivity and therefore the electrical characteristics.

2.2 Electrical analysis without the ion-selective membranes

The configuration employed for testing the DMSO-treated OECTs is shown in the inset of **Figure 2**a and in Figure S1a, with a poly(methyl methacrylate) (PMMA) reservoir integrated to the PI foil to confine the Phosphate-Buffered Saline (PBS) solution. The electrical testing includes drain current-gate voltage (I_{ds}-V_{gs}) measurements in Figure 2a,c and drain current-drain voltage (I_{ds}-V_{ds}) measurements in Figure 2b, with hysteresis and leakage current. The OECTs exhibit a transconductance, g_m ($\Delta I_{ds}/\Delta V_{gs}$), of 247 ± 24 μS for the same printed batch (n=3) and 238 ± 129 μS for multiple printed batches (4 batches, n=8), with a peak close to 0 V (Figure 2a). Such variability is common for inkjet-printed polymers, due to some variations in thickness and uniformity of the printed organic layers, affecting the electrical resistance of the channel and the related transconductance. Considering the design parameters, with a width to

length ratio equal to 0.3 and a thickness of ~100 nm, the reported transconductance values are comparable with lithographically-patterned OECTs.[33,42] The ON-OFF ratio of the devices is ~60 (n=3). As expected, we observe an increase of the leakage current with the gate voltage applied (Figure 2c), likely due to the silver gate oxidation in the presence of chloride ions.[56]

To further investigate the influence of ions at the organic channel and the gate electrode interfaces, electrical measurements at different ionic concentrations in the range of 1–50 mM (Figure 2d-f) are performed. When the concentration of potassium chloride (KCl) increases, a shift of the curve towards a lower drain current is observed, while the response in DI water ($<10^{-6}$ M) is quasi-flat (Figure 2d). Figure 2e and Figure 2f show, respectively, the I_{ds} and I_{gs} variations in time upon the addition of multiple concentrations of NaCl and KCl, with the gate and the drain voltages fixed. The leakage current I_{gs}, probably due to the variations of potential on the gate electrode at different chloride concentrations,[56] is much smaller (>100X less) compared to the I_{ds} values in Figure 2e. Hence, according to the device physics,[29] since the I_{ds} current depends on the cations injection, we can conclude that there is a negligible effect of chloride on the sensing response.

2.3 Electrical analysis with the ion-selective membranes

As previously shown in Figure 2e, monovalent ions such as sodium and potassium have the same effect in the de-doping of the organic polymer, thus requiring the use of a specific ion-selective membrane for being differentiated. In this study, we prepared ISMs based on valinomycin, sodium ionophore X, and hydrogen ionophore I in polyvinyl chloride (PVC) matrices, to achieve selectivity for K^+, Na^+, and H^+ ions, respectively. These three cases of interest are depicted in **Figure 3**: With the use of an optimized ISM, the number of ions present in the electrolyte that can dynamically interact with the underlying PEDOT:PSS layer, and electrostatically compensate the PSS negative charges, should be considerably less. Hence, the polarons (holes) de-doping is dependent on the selective membrane (Figure 3d-f).

However, the thickness of the drop-casted ISM on standard ion-selective electrodes can reach hundreds of micrometers, depending on the electrode area and solution volume.[57] Such thick membranes can significantly hinder the transistor response, which is typically within few milliseconds thanks to the extremely thin active layer.[58] To investigate this effect, the three different ISMs are cast on the organic layers of the transistors with two thicknesses and tested in a PBS solution with a fixed concentration of sodium and potassium at pH 7. The volume of the membranes was ~2 μL and ~5 μL for each ISM, fully covering the PEDOT:PSS layer, resulting in an average thickness of deposited material equal to 33 ± 7 μm (n=9) or 54 ± 15 μm (n=7), respectively. The electrical characteristics of devices with thinner membranes are shown in **Figure 4**a-c while those for thicker membranes are presented in Figure 4d-e. The thin membrane led to a better transistor modulation (Figure 4a) compared to the thicker one (Figure 4d), with a transconductance shift of 0.1–0.4 V with respect to 0.4 V–0.7 V. The larger g_m shift for the thick membranes can be explained by the lower membrane permeability, leading to fewer ions reaching the PEDOT:PSS layers. Such an effect can be compensated by a higher gate voltage, resulting in stronger ions injection. Besides, this results in similar transconductance values for no-membrane and thin-membranes (Figure 4b) devices, while a three-fold g_m decrease is observed for thick-membrane devices (Figure 4e). The time response (τ) of the devices was extracted by fitting their response curves in Figure 4c,f with an exponential decay function. The values are equal to 5.75 ± 0.25 s (n=2) for devices without any membrane, increasing with the sodium and potassium membranes to 12 ± 4 s (n=2) for the thin membranes (2.11X increase), and 25 ± 7 s (n=2) for the thick membranes (4.35X increase). The H^+ sensor shows a relatively faster response, which is less influenced by the membrane thickness, with values equal to 6.5 s for the thin membrane and 7.5 s for the thick membrane (Figure 4f), due possibly to higher penetration of the ions. The measured current changes can

be due to the previously mentioned variability related to the printing process, and further comparisons will be done in the next section particularly considering the normalized sensitivity.

2.4 Array integration into the microfluidic system and sensing

The OECTs with the thinner ion-selective membranes are integrated into a PET microfluidics system as shown in Figure 1a,b. This integrated flexible platform, with four transistors included, is used for measuring in time ionic solutions at different physiologically relevant concentrations, performing sensitivity (**Figure 5**a-d) and selectivity (Figure 5e-h) tests. Ionic solutions of 1–100 mM are made with KCl or NaCl dissolved in DI water, while pH buffer solutions in the range of 4–7 are employed for the pH measurements.

For the sensitivity analysis (Figure 5a-d), the ions are injected in the microfluidics inlet from a low to a high and subsequently high to low concentration. DI water is used as a baseline solution when starting and finishing all the tests. A measurement without any selective membrane is presented in Figure 5a. All the sensors exhibit very good stability in time with low drift for the time of the measurements. The sensitivity, proportional to the logarithmic of the concentrations (Figure S5), is extracted from the steady-state response after each injection. The value is equal to 18 ± 2 μA dec^{-1} for devices without any membrane, 7.5 ± 1.5 μA dec^{-1} with the K^+ membrane, 6.5 ± 0.5 μA dec^{-1} with the Na^+ membrane (to KCl or NaCl concentrations, respectively), and 11 ± 1 μA pH^{-1} with the H^+ membrane. The sensitivity values are averaged from two devices coming from the same printed batch. The sodium and potassium sensors show reversibility from low to high and high to low concentrations. With the H^+ membrane, the devices present instability when starting and finishing the measurements in DI water, likely due to the non-negligible ionic strength of the solution (Fig. 5d,h).

Most importantly, the selectivity of the OECTs with ISMs is clearly shown from the ionic measurements in time (Figure 5e-h). The OECTs without any membrane have almost the same

responses towards KCl and NaCl changes in concentration (Figure 5e), while the transistors with the ISMs show a much smaller response towards the respective tested interfering ion (Figure 5f,g). At a high concentration of salt equal to 100 mM, from the division of the signal obtained for the non-interfering ions by the signal for the interfering ions, a 12X higher signal towards K^+ to Na^+ with K^+-ISM and a 3X higher signal towards Na^+ to K^+ with Na^+-ISM were extracted. Considering the pH measurements, the selectivity test is performed adding a background of different salt concentrations at a fixed pH buffer solution (Figure 5h). The signal measured for a pH 4 buffer resulted to be 2X higher than the signal from the highly concentrated background (100 mM) in the pH 7 buffer, calculated starting from the same buffer solution without ions being added.

To analyze the reproducibility among the printed devices, a normalized sensitivity was extracted for four devices of each type and coming from two different fabrication batches (Figure S6). The normalized sensitivity, calculated as the absolute value of $\frac{I_{response}-I_{baseline}}{I_{baseline}} x\ 100$, was of 23 ± 0.7 %·dec^{-1} without the membrane, 29 ± 3 %·dec^{-1} with the K^+ membrane, 13 ± 3 %·dec^{-1} with the Na^+ membrane, and 28 ± 4 %·dec^{-1} with H^+ membrane, extracted using DI water as a baseline for Na^+, K^+, and neutral pH buffer for H^+. It can be concluded that all types of sensing devices exhibit a small variation of their sensitivity, confirming the reproducibility of the fabrication approach. It can be noticed that for the Na^+ sensor the normalized sensitivity is smaller than the others, possibly due to a lower ion permeability of the membrane.

3. Conclusions

In summary, we have demonstrated a flexible platform of inkjet-printed sensing transistors with the PEDOT:PSS active layers coated with three different ion-selective membranes. In comparison to literature, in which the ISM were suspended above inner filling solutions,[59] or

gels,[2] in bulky reservoirs, here the ISMs are directly cast on the organic channel. By adding a small volume of the membrane and having enhanced membrane permeability, a minimum impact on the device performances in terms of transfer characteristics and time response is achieved while providing high ion selectivity. The multiple ion-selective electrochemical transistors are also integrated into a flexible microfluidics system. This novel platform allows real-time, multi-ion sensing with low cross-sensitivity. The OECTs selectivity is proven in real-time, extracting a 12X higher signal towards potassium to sodium with the K^+-ISM, a 3X higher signal towards sodium to potassium with the Na^+-ISM, and a 2X higher signal towards H^+ to a high salt background with the H^+-ISM. All the ion-selective sensors exhibit a sensitivity of ~10 μA dec^{-1} with good stability for the time of the measurements. However, the H^+ sensor linearity and selectivity should be further improved, potentially by implementing an active-gate material such as polyaniline.[36] Proof of reproducibility is demonstrated in terms of normalized sensitivity among two different printed batches.

A summary table comparing our OECTs with the literature is reported in the Supplementary (Table S1). The ion-selective devices in this work have a 20X higher sensitivity than reported lithographically-patterned ion-selective EGOFETs (Electrolyte-Gated Organic Field-Effect Transistors).[59] They also show sensitivities comparable to lithographically patterned OECTs on glass substrates without,[60] and with a suspended ISM,[2] all within the order of tens of μA dec^{-1}. Their sensitivity could be further improved by modifying the proposed design of the OECTs, such as by increasing the W/L ratio, which would result in an increase of their transconductance. Finally, for the first time, these sensing capabilities are combined with a high level of integration and a simple fabrication with digitally manufacturing technologies, to have a low cost, wearable, and multi-sensing platform. Our OECTs could be further scaled down, integrating more sensors into a smaller microfluidic system, with minimal sample volume required, hence enabling real-time multi-electrolytes monitoring in everyday life.

Available at: https://doi.org/10.1002/admt.202000328

4. Experimental Section

Fabrication and layers characterization: The fabrication was performed with a Dimatix DMP printer (Fujifilm) using the 10 pL cartridges. The PEDOT:PSS (1 S/cm, 1.3 wt % dispersion in H_2O, Sigma Aldrich) and the silver nanoparticle (PV Nano Cell) inks were sonicated for 5 minutes and subsequently filtered with a 0.2 μm pore-size filter when filling the respective cartridges. The polyimide substrate (125 μm-thick) was treated with oxygen plasma before printing. The Dimatix substrate holder was kept at 40 °C. The process started with the printing of 2 layers of the silver gate, source and drain electrodes and subsequent sintering at 150 °C for 1 hour. Then, the PEDOT:PSS layers were printed (1 to 4 layers), post-treated by dispersing dimethyl sulfoxide (DMSO) solvent fully covering the PEDOT:PSS film and subsequently cured at 120 °C for 20 minutes. The OECTs were designed to be simple to integrate as an array into the microfluidics while limiting as well the ON-current for future portable implementations at low power. All the electrical resistance measurements were performed using a multimeter connected between the drain and source contacts of the PEDOT:PSS. The thicknesses measurements were performed using a laser scanning microscope (Keyence VK-X1000 Series), with 50X and 10X magnification for the PEDOT:PSS layers and the membranes, respectively. The thickness measurements were confirmed with the Wyko NT1100 (Veeco) and the profilometer Alphastep IQ (Tencor).

Membranes preparation: All the chemicals have been purchased from Sigma Aldrich unless otherwise stated. The H^+ ion-selective membrane was prepared by dissolving hydrogen I ionophore (1.92 mM), potassium tetrakis(4-chlorophenyl)borate (1.01 mM), bis(2-ethylhexyl)sebacate (153.51 mM), and polyvinyl chloride (3.3 wt/vol%) in tetrahydrofuran. The solution was thoroughly mixed for 1 hour to get a homogenous membrane. For the Na^+ membrane, sodium ionophore X (1.5 mM), sodium tetrakis[3,5-bis(trifluoromethyl)phenyl]borate (0.940 mM), bis(2-ethylhexyl) sebacate (232.420 mM),

and polyvinyl chloride (5 wt/vol%) were dissolved in tetrahydrofuran by thoroughly mixing until getting a transparent solution. Finally, the K^+ membrane was prepared by dissolving potassium ionophore valinomycin (5.142 mM), sodium tetraphenyl boron (4.174 mM), bis(2-ethylhexyl) sebacate (433.25 mM), and polyvinyl chloride (9.371 wt/vol %) in cyclohexanone. The prepared K^+ solution was thoroughly mixed for 1 hour to get a homogenous mixture. All the prepared solutions were stored at 4 °C. The membranes were drop-cast on the organic layer before the insulation of the drain-source contacts, to avoid the confinement of the membrane. After casting, a drop of 100 mM KCl or NaCl solution in DI water was left on the K^+ or Na^+ membrane respectively, and a drop of pH 4 buffer on the H^+ membrane, to stabilize the membrane for one hour. The sensors were washed with DI water before the sensing experiments.

Ionic solutions: For the pH sensing tests, buffer concentrate solutions (Titrisol) were employed. For potassium and sodium sensing tests, NaCl (Sigma Aldrich) and KCl (Merck) were used and dissolved in DI water. The basic PBS 1X solution was made using monopotassium phosphate (KH_2PO_4 from Merck, 1 mM), NaCl (155 mM), and disodium phosphate (Na_2HPO_4 from Merck, 2.966 mM). For the experiments related to the effect of the membrane thickness on the OECTs electrical characteristics, KCl (155 mM) was added to the previous mixture.

Microfluidics fabrication: A PET foil (125 μm-thick) was used for the flexible fluidics system. The foil was patterned by CO_2 laser etching (Trotec Speedy300 laser cutter) to define the shape of the micro-fluidic channel, the reservoir, the inlet and the outlet. The PET fluidics system was made by lamination of the patterned PET layer with a PET top cover, bonded using a double-side silicone adhesive (ARclear 8932EE). The adhesive was used also to fix the fluidics system to the organic transistor arrays on polyimide.

Characterization and data analysis: The OECTs were tested by either injection of the electrolyte solutions in the microfluidics system or confining the solution in PMMA reservoirs, fixed using the double-sided ARclear adhesive. The PMMA reservoirs were laser cut using the

CO_2 laser with the adhesive laminated before the cutting. The OECTs source and drain contacts, close to the PEDOT:PSS layer, were insulated using a transparent dielectric to avoid the electrolyte to be in contact with the silver electrodes. The measurements at different ionic concentrations with the PMMA reservoirs were performed starting from 10 μL DI water and subsequently adding 10 μL solutions at different concentrations (1–50 mM). Before performing sensing measurements with the microfluidics system, I_{ds}-V_{gs} characteristics in PBS 1X were acquired for each sensor and repeated five times, to extract the voltage at the peak of transconductance and stabilize the signal. The sensors were then washed three times by injections of 1 ml DI water. The sensing in microfluidics was performed with injections using a syringe (~0.4 ml solution for injection). The testing was performed with the different ISMs on the same array, measuring one device of the fully functionalized OECTs array at the time and switching between devices. All the OECTs electrical measurements were acquired using a semiconductor parameter analyzer (Agilent 4155A), with an integration time of 20 ms (medium) or 320 ms (long). The data were analyzed with the software Origin 2019b.

Supporting Information

Supporting Information is available from the Wiley Online Library or from the author.

Acknowledgements

The authors gratefully acknowledge the funding from SNF-SINERGIA under the project WeCare (N°CRSII5_177255) and SNF under the project 206021:164028: "Aerosol Jet Tool for Additive Manufacturing and 3D Printing for Microsystems". The authors wish to thank Dr. Peter van der Wal for the useful advice on the ion-selective membranes preparation and electrochemical analysis, Dr. Alexis Marette for the initial support on inkjet printing of the OECTs and Dr. Jaemin Kim for his help with the 3D images. Special thanks to Dr. Giorgio Mattana, Prof. Benoit Piro, Prof. Vincent Noël, and Dr. Khalil Chennit for the useful discussions on organic transistors.

Conflict of interest

The authors declare no conflict of interest.

Received: ((will be filled in by the editorial staff))
Revised: ((will be filled in by the editorial staff))
Published online: ((will be filled in by the editorial staff))

Available at: https://doi.org/10.1002/admt.202000328

References

[1] W. Gao, S. Emaminejad, H. Y. Y. Nyein, S. Challa, K. Chen, A. Peck, H. M. Fahad, H. Ota, H. Shiraki, D. Kiriya, D. H. Lien, G. A. Brooks, R. W. Davis, A. Javey, *Nature* **2016**, *529*, 509.

[2] M. Sessolo, J. Rivnay, E. Bandiello, G. G. Malliaras, H. J. Bolink, *Adv. Mater.* **2014**, *26*, 4803.

[3] M. Bariya, H. Y. Y. Nyein, A. Javey, *Nat. Electron.* **2018**, *1*, 160.

[4] A. J. Bandodkar, J. Wang, *Trends Biotechnol.* **2014**, *32*, 363.

[5] D. Vairo, L. Bruzzese, M. Marlinge, L. Fuster, N. Adjriou, N. Kipson, P. Brunet, J. Cautela, Y. Jammes, G. Mottola, S. Burtey, J. Ruf, R. Guieu, E. Fenouillet, *Sci. Rep.* **2017**, *7*, 1.

[6] J. Kim, A. S. Campbell, B. E. F. de Ávila, J. Wang, *Nat. Biotechnol.* **2019**, *37*, 389.

[7] Y. Kim, T. Lim, C. H. Kim, C. S. Yeo, K. Seo, S. M. Kim, J. Kim, S. Y. Park, S. Ju, M. H. Yoon, *NPG Asia Mater.* **2018**, *10*, 1086.

[8] H. Y. Y. Nyein, M. Bariya, L. Kivimäki, S. Uusitalo, T. S. Liaw, E. Jansson, C. H. Ahn, J. A. Hangasky, J. Zhao, Y. Lin, T. Happonen, M. Chao, C. Liedert, Y. Zhao, L. C. Tai, J. Hiltunen, A. Javey, *Sci. Adv.* **2019**, *5*, 1.

[9] M. Ghittorelli, L. Lingstedt, P. Romele, N. I. Cra, Z. M. Kovács-vajna, P. W. M. Blom, F. Torricelli, *Nat. Commun.* **2018**, *9*, 1.

[10] L. B. Baker, K. A. Barnes, M. L. Anderson, D. H. Passe, J. R. Stofan, *J. Sports Sci.* **2016**, *34*, 358.

[11] G. Palacios, R. Pedrero-Chamizo, N. Palacios, B. Maroto-Sanchez, S. Aznar, M. Gonzalez-Gross, *Nutr. Hosp.* **2015**, *31*, 237.

[12] R. A. Neal, H. C. Massey, M. J. Tipton, J. S. Young, J. Corbett, *Front. Physiol.* **2016**, *7*, 1.

[13] N. L. Nelson, J. R. Churilla, *Muscle and Nerve* **2016**, *54*, 177.

[14] B. Lara, J. J. Salinero, F. Areces, D. Ruiz-Vicente, C. Gallo-Salazar, J. Abián-Vicén, J. Del Coso, *Scand. J. Med. Sci. Sport.* **2015**, 1.

[15] D. A. Sakharov, M. U. Shkurnikov, M. Y. Vagin, E. I. Yashina, A. A. Karyakin, A. G. Tonevitsky, *Bull. Exp. Biol. Med.* **2010**, *150*, 94.

[16] Z. Sonner, E. Wilder, J. Heikenfeld, G. Kasting, F. Beyette, D. Swaile, F. Sherman, J. Joyce, J. Hagen, N. Kelley-Loughnane, R. Naik, *Biomicrofluidics* **2015**, *9*, 1.

[17] T. Someya, Z. Bao, G. G. Malliaras, *Nature* **2016**, *540*, 379.

[18] A. Pierre, S. E. Doris, R. Lujan, R. A. Street, *Adv. Mater. Technol.* **2019**, *4*, 1.

[19] C. Liao, C. Mak, M. Zhang, H. L. W. Chan, F. Yan, *Adv. Mater.* **2015**, *27*, 676.

[20] L. Nela, J. Tang, Q. Cao, G. Tulevski, S. J. Han, *Nano Lett.* **2018**, *18*, 2054.

[21] C. Wu, J. Selberg, B. Nguyen, P. Pansodtee, M. Jia, H. Dechiraju, M. Teodorescu, M. Rolandi, *Small* **2020**, *16*, 1.

[22] S. Zhang, H. Ling, Y. Chen, Q. Cui, J. Ni, X. Wang, M. C. Hartel, X. Meng, K. J. Lee, J. Lee, W. Sun, H. Lin, S. Emaminejad, S. Ahadian, N. Ashammakhi, M. R. Dokmeci, A. Khademhosseini, *Adv. Funct. Mater.* **2020**, *30*, 1.

[23] A. Tricoli, N. Nasiri, S. De, *Adv. Funct. Mater.* **2017**, *27*, 1.

[24] M. Cuartero, M. Parrilla, G. A. Crespo, *Sensors* **2019**, *19*, 1.

[25] E. Zdrachek, E. Bakker, *Anal. Chem.* **2019**, *91*, 2.

[26] T. Guinovart, G. A. Crespo, F. X. Rius, F. J. Andrade, *Anal. Chim. Acta* **2014**, *821*, 72.

[27] V. A. T. Dam, M. Goedbloed, M. A. G. Zevenbergen, *Eurosensors Conf. Paris, Fr.* **2017**, *1*, 464.

[28] I. Gualandi, M. Tessarolo, F. Mariani, D. Tonelli, B. Fraboni, E. Scavetta, *Front. Bioeng. Biotechnol.* **2019**, *7*, 1.

[29] J. Rivnay, S. Inal, A. Salleo, M. Berggren, G. G. Malliaras, *Nat. Rev. Mater.* **2018**, *3*, 1.

[30] K. Tybrandt, I. V Zozoulenko, M. Berggren, *Sci. Adv.* **2018**, *3*, 1.

[31] L. Kergoat, B. Piro, D. T. Simon, M. C. Pham, V. Noël, M. Berggren, *Adv. Mater.* **2014**, *26*, 5658.

[32] S. Savagatrup, E. Chan, S. M. Renteria-Garcia, A. D. Printz, A. V. Zaretski, T. F. O'Connor, D. Rodriquez, E. Valle, D. J. Lipomi, *Adv. Funct. Mater.* **2015**, *25*, 427.

[33] J. Rivnay, P. Leleux, M. Ferro, M. Sessolo, A. Williamson, D. A. Koutsouras, D. Khodagholy, M. Ramuz, X. Strakosas, R. M. Owens, C. Benar, J. M. Badier, C. Bernard, G. G. Malliaras, *Sci. Adv.* **2015**, *1*, 1.

[34] P. Romele, M. Ghittorelli, Z. M. Kovács-Vajna, F. Torricelli, *Nat. Commun.* **2019**, *10*, 1.

[35] A. V. Volkov, K. Wijeratne, E. Mitraka, U. Ail, D. Zhao, K. Tybrandt, J. W. Andreasen, M. Berggren, X. Crispin, I. V. Zozoulenko, *Adv. Funct. Mater.* **2017**, *27*, 1.

[36] G. Scheiblin, R. Coppard, R. M. Owens, P. Mailley, G. G. Malliaras, *Adv. Mater. Technol. 2017*, **2017**, *2*, 1.

[37] N. Coppedè, M. Giannetto, M. Villani, V. Lucchini, E. Battista, M. Careri, A. Zappettini, *Org. Electron.* **2020**, *78*, 1.

[38] R. Faddoul, R. Coppard, T. Berthelot, *Proc. IEEE Sensors* **2014**, 1088.

[39] S. Demuru, A. Marette, W. Kooli, P. Junier, D. Briand, *Proc. Eurosensors - Transducers* **2019**, *1*, 2519.

[40] T. Carey, S. Cacovich, G. Divitini, J. Ren, A. Mansouri, J. M. Kim, C. Wang, C. Ducati, R. Sordan, F. Torrisi, *Nat. Commun.* **2017**, *8*, 1.

[41] T. Blaudeck, P. A. Ersman, M. Sandberg, S. Heinz, A. Laiho, J. Liu, I. Engquist, M. Berggren, R. R. Baumann, *Adv. Funct. Mater.* **2012**, *22*, 2939.

[42] S. Inal, G. G. Malliaras, J. Rivnay, *Nat. Commun.* **2017**, *8*, 1.

[43] D. Khodagholy, J. Rivnay, M. Sessolo, M. Gurfinkel, P. Leleux, L. H. Jimison, E. Stavrinidou, T. Herve, S. Sanaur, R. M. Owens, G. G. Malliaras, *Nat. Commun.* **2013**, *4*, 1.

[44] Y. Liang, F. Brings, V. Maybeck, S. Ingebrandt, B. Wolfrum, A. Pich, A. Offenhäusser, D. Mayer, *Adv. Funct. Mater.* **2019**, *29*, 1.

[45] M. Braendlein, A. M. Pappa, M. Ferro, A. Lopresti, C. Acquaviva, E. Mamessier, G. G. Malliaras, R. M. Owens, *Adv. Mater.* **2017**, *29*, 1.

[46] F. Mariani, I. Gualandi, M. Tessarolo, B. Fraboni, E. Scavetta, *ACS Appl. Mater. Interfaces* **2018**, *10*, 22474.

[47] S. T. Keene, A. Marais, V. F. Curto, A. Salleo, O. Parlak, *Sci. Adv.* **2018**, *4*, 1.

[48] E. Bihar, Y. Deng, T. Miyake, M. Saadaoui, G. G. Malliaras, M. Rolandi, *Sci. Rep.* **2016**, *6*, 2.

[49] M. Sessolo, J. Rivnay, E. Bandiello, G. G. Malliaras, H. J. Bolink, *Adv. Mater.* **2014**, *26*, 4803.

[50] Z. Mousavi, A. Ekholm, J. Bobacka, A. Ivaska, *Electroanalysis* **2009**, *21*, 472.

[51] S. T. Keene, D. Fogarty, R. Cooke, C. D. Casadevall, A. Salleo, O. Parlak, *Adv. Healthc. Mater.* **2019**, *8*, 1.

[52] T. R. Chou, S. H. Chen, Y. Te Chiang, Y. T. Lin, C. Y. Chao, *Mol. Cryst. Liq. Cryst.* **2015**, *612*, 201.

[53] Y. Liu, J. J. S. Norton, R. Qazi, Z. Zou, K. R. Ammann, H. Liu, L. Yan, P. L. Tran, K. I. Jang, J. W. Lee, D. Zhang, K. A. Kilian, S. H. Jung, T. Bretl, J. Xiao, M. J. Slepian, Y. Huang, J. W. Jeong, J. A. Rogers, *Sci. Adv.* **2016**, *2*, 1.

[54] L. V Lingstedt, M. Ghittorelli, H. Lu, D. A. Koutsouras, T. Marszalek, F. Torricelli, N. I. Cra, P. W. M. Blom, *Adv. Electron. Mater.* **2019**, *5*, 1.

[55] S. Kim, B. Sanyoto, W. T. Park, S. Kim, S. Mandal, J. C. Lim, Y. Y. Noh, J. H. Kim, *Adv. Mater.* **2016**, *28*, 10149.

[56] G. Tarabella, C. Santato, S. Y. Yang, S. Iannotta, G. G. Malliaras, F. Cicoira, *Appl. Phys. Lett.* **2010**, *97*, 1.

[57] K. Xu, M. Cuartero, G. A. Crespo, *Sensors Actuators, B Chem.* **2019**, *297*, 1.

Available at: https://doi.org/10.1002/admt.202000328

[58] J. T. Friedlein, M. J. Donahue, S. E. Shaheen, G. G. Malliaras, R. R. McLeod, *Adv. Mater.* **2016**, *28*, 8398.

[59] K. Schmoltner, J. Kofler, A. Klug, E. J. W. List-Kratochvil, *Adv. Mater.* **2013**, *25*, 6895.

[60] P. Lin, F. Yan, H. L. W. Chan, *ACS Appl. Mater. Interfaces* **2010**, *2*, 1637.

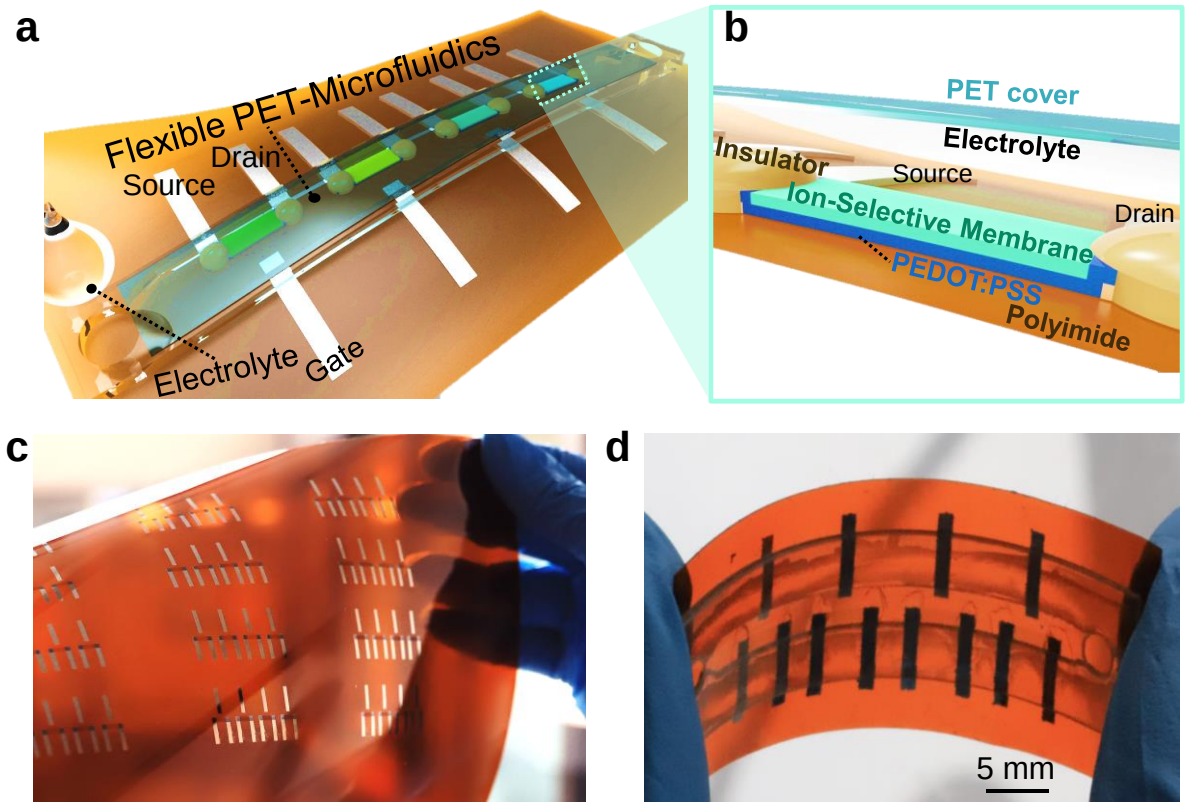

Figure 1. a) Schematic of the integrated organic transistors into the microfluidic system and zoom with the cross-section in (b). c,d) Images of the transistors, without and with microfluidics in (c) and (d), respectively.

Available at: https://doi.org/10.1002/admt.202000328

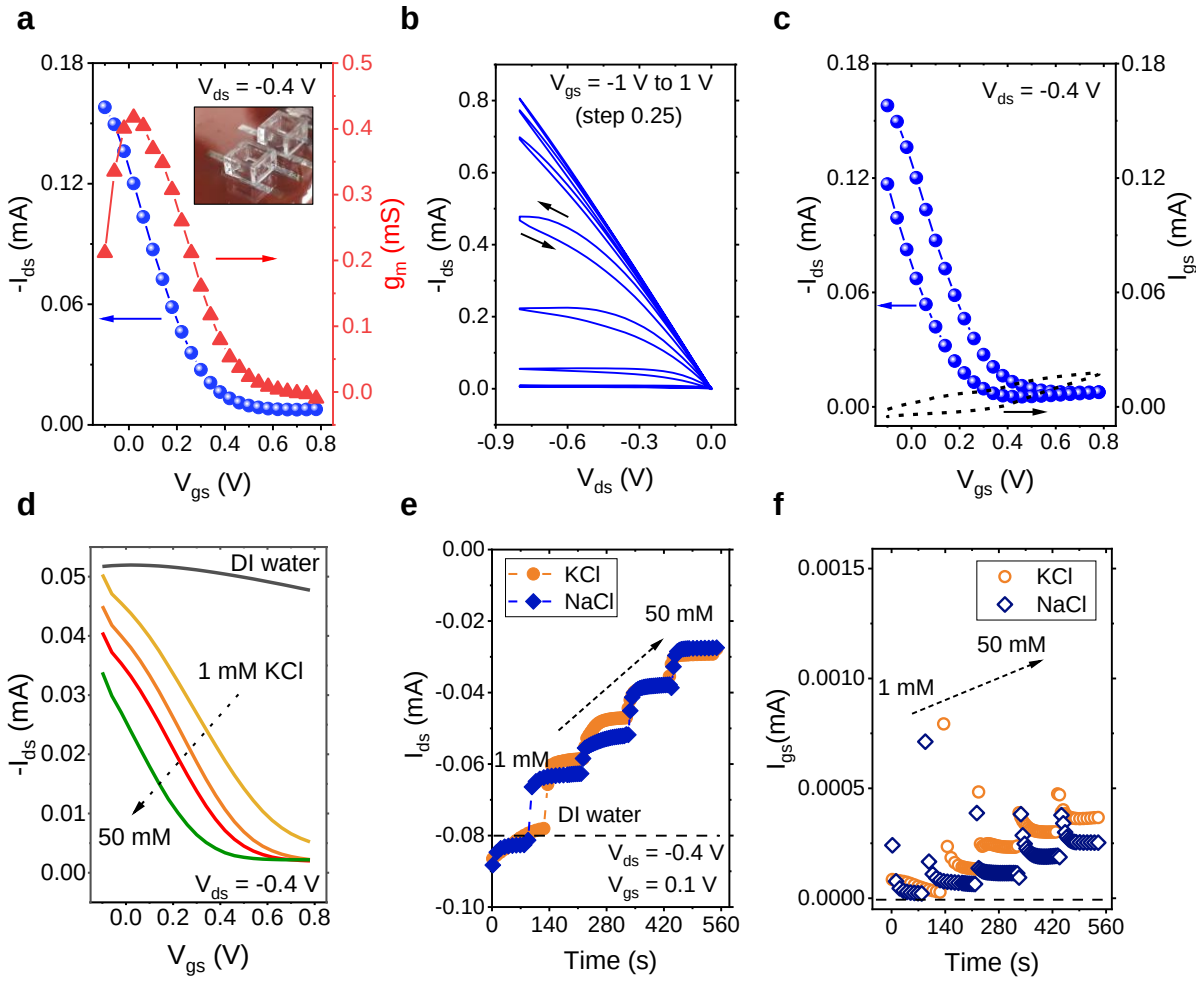

Figure 2. a-c) The electrical characteristics of the DMSO treated OECT in PBS 1X (0.155 M NaCl, pH 7). d) Transfer curves at different ionic concentrations of KCl including DI water as a baseline. e) Time measurements with different ionic solutions and concentrations. f) Leakage current with different ionic solutions and concentrations.

Available at: https://doi.org/10.1002/admt.202000328

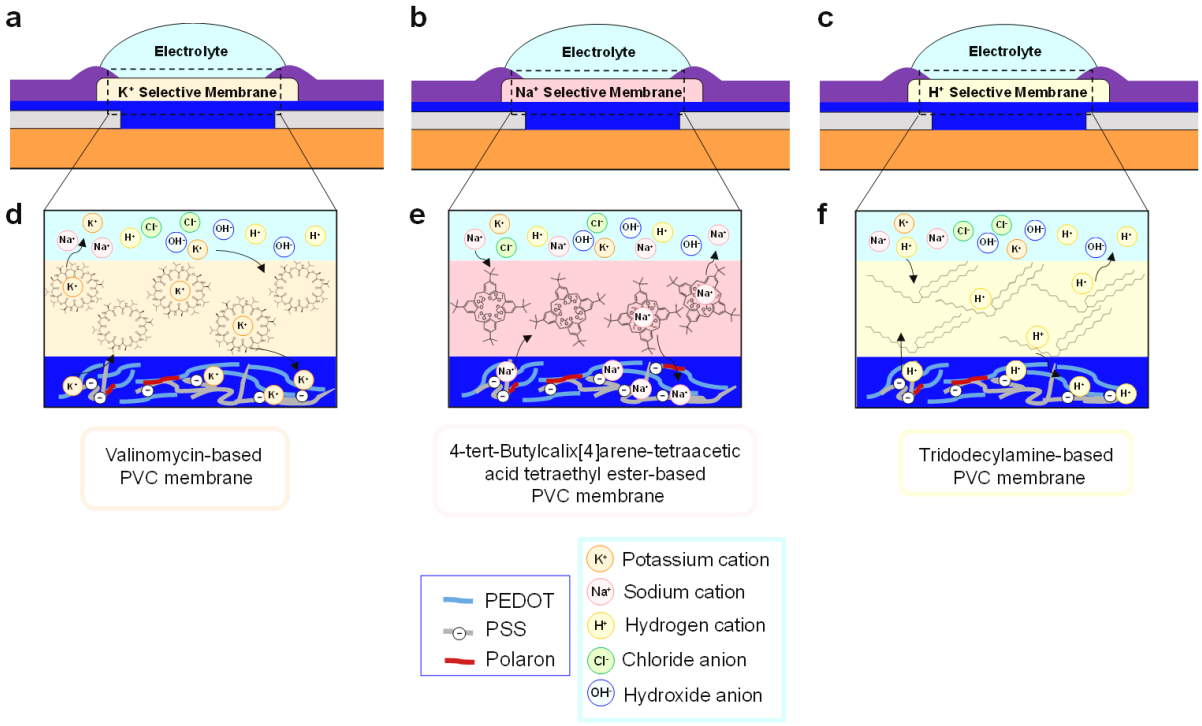

Figure 3. a-c) Sketches of OECTs with different ion-selective membranes. d-f) Simplified interactions between an electrolyte solution, the ion-selective membranes, and the PEDOT:PSS active layer considering (d) the potassium ionophore-based membrane, (e) the sodium ionophore X-based membrane and (f) the hydrogen ionophore I-based membrane. The chemical name of the respective ionophore is reported in the image. The sulfonate groups and the polarons (holes) of the organic layers are also represented, with the respective permeated ions de-doping the PEDOT by removing the polarons.

Available at: https://doi.org/10.1002/admt.202000328

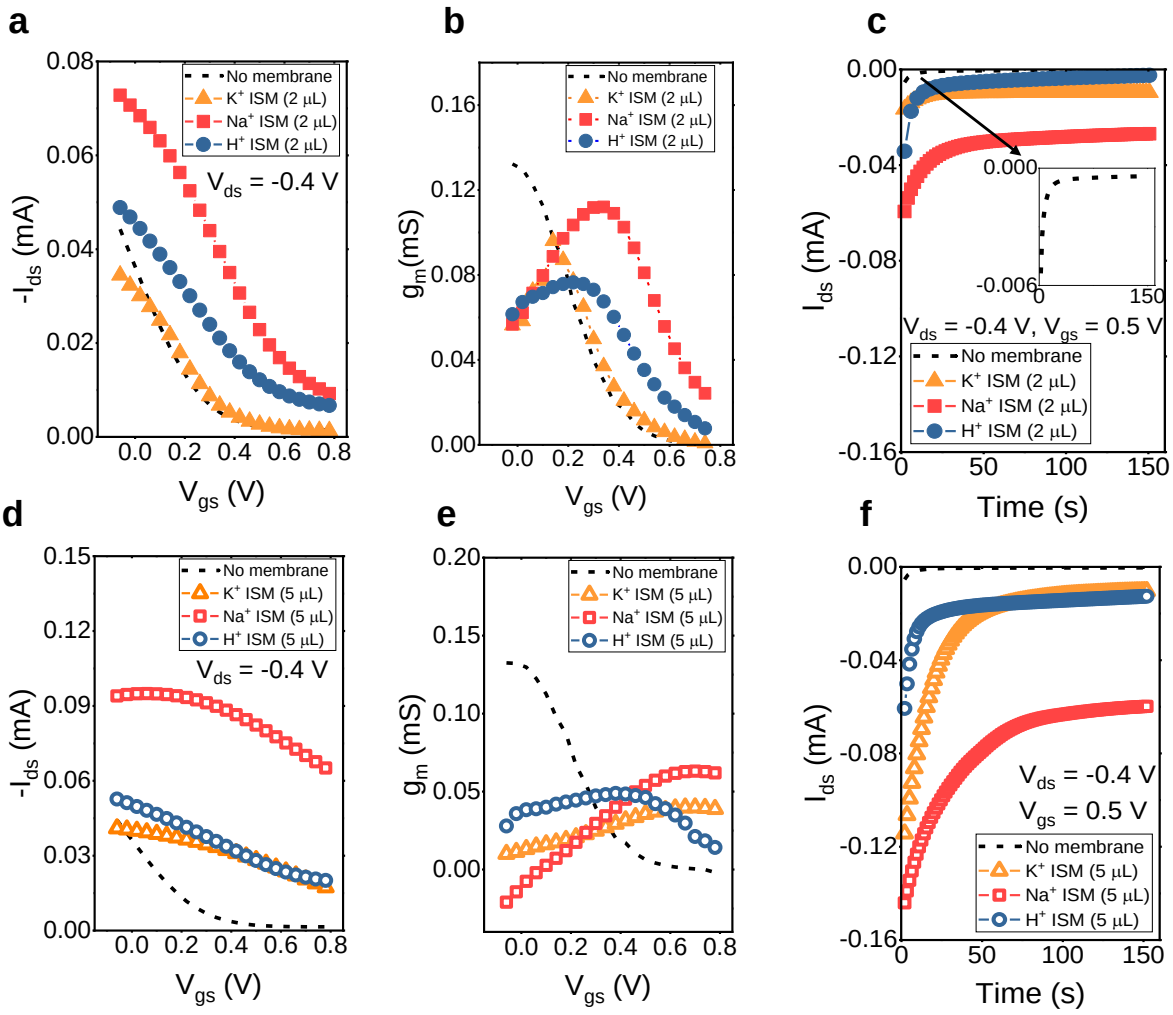

Figure 4. Organic transistors electrical responses in PBS (0.155 M NaCl + 0.155 M KCl, pH 7) with (a-c) lower (~2 µL**)** and (d-f) higher **(**~5 µL**)** volume of the three different ion-selective membranes. The results are compared to a bare device (no membrane). The analysis includes transfer characteristics in (a,d), transconductance in (b,e) and time response in (c,f). The integration time was 320 ms in all cases.

Available at: https://doi.org/10.1002/admt.202000328

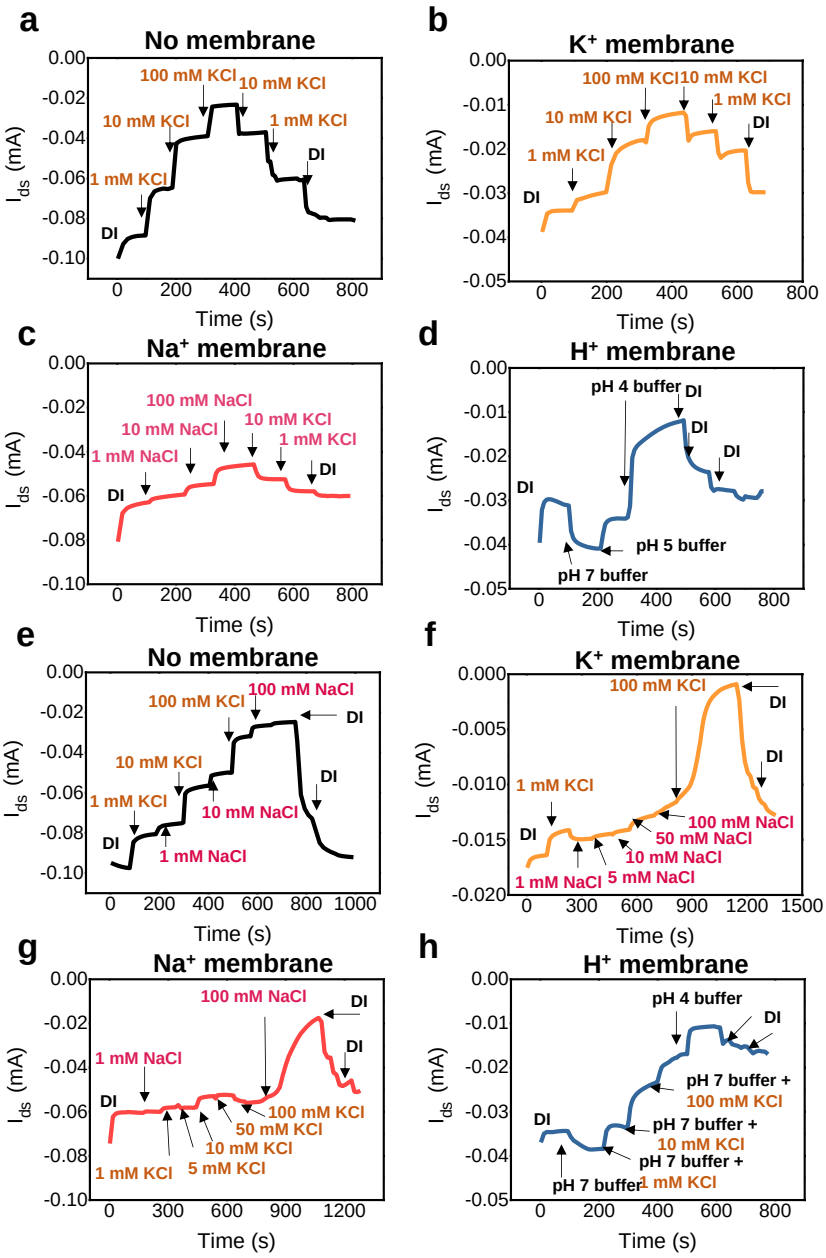

Figure 5. Ion sensing with the integrated microfluidic system for OECTs without a membrane in (a,e), with the K^+ selective membrane in (b,f), the Na^+ selective membrane in (c,g), and the H^+ selective membrane in (d,h). The sensitivity tests are shown in (a-c) and the selectivity tests in (e-h). The solutions (except the pH buffers) were made with KCl or NaCl dissolved in DI water. V_{ds}= -0.4 V, while V_{gs} was fixed close to the transconductance peak (0.1-0.4 V) for each device.

Available at: https://doi.org/10.1002/admt.202000328

Table of contents

An integrated array of inkjet-printed flexible organic electrochemical transistors that perform real-time, sensitive and selective detection of potassium (K^+), sodium (Na^+), and hydrogen (H^+) ions at physiologically relevant sweat concentrations is demonstrated. The thin-film transistors with multiple ion-selective membranes (ISMs) are integrated into a flexible microfluidics system, enabling continuous measurements of electrolytes in body fluids.

Keyword Wearable Ion Sensors

Silvia Demuru, Brince Paul Kunnel, and Danick Briand**

Real-Time Multi-Ion Detection in the Sweat Concentration Range Enabled by Flexible, Printed and Microfluidics-Integrated Organic Transistor Arrays

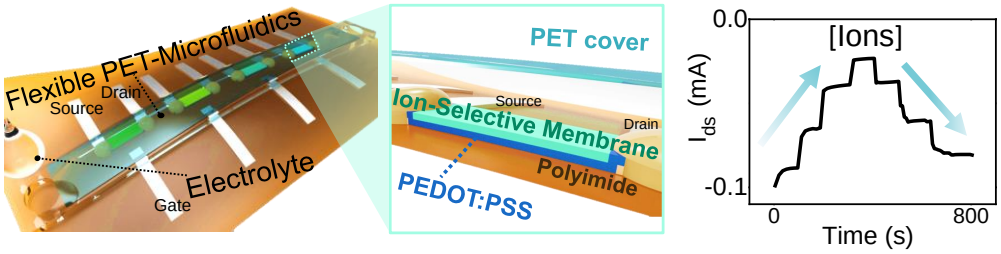

ToC Figure